Structural and magnetic study of $LaBaCoCuO_{5+\delta}$

Leopoldo Suescun,[1] Camille Y. Jones,[2] Claudio A. Cardoso,[3] Jeffrey W. Lynn,[2] Brian H. Toby,[2]
Fernando M. Araújo-Moreira,[3] Oscar F. de Lima,[4] Helena Pardo,[1] and Alvaro W. Mombrú[1,*]
[1]*Crystallography, Solid State and Materials Laboratory (Cryssmat-Lab), Dequifim, Facultad de Química, Universidad de la República, P.O. Box 1157, Montevideo, Uruguay*
[2]*NIST Center for Neutron Research, National Institute of Standards and Technology, Gaithersburg, Maryland 20899-8562, USA*
[3]*Grupo de Materiais e Dispositivos, CMDMC, Departamento de Física, Universidade Federal de São Carlos, UFSCar, Caixa Postal 676, 13565-905 São Carlos, São Paulo, Brazil*
[4]*Instituto de Física "Gleb Wataghin," UNICAMP, 13083-970 Campinas, São Paulo, Brazil*
(Received 4 October 2004; revised manuscript received 14 December 2004; published 12 April 2005)

The structure and magnetic properties of the compound $LaBaCuCoO_{5+\delta}$ have been studied for the non-stoichiometric oxygen concentration $\delta \approx 0.6$. The structure is pseudo-cubic with a tripled perovskite unit cell. The crystal structure was determined by a combined Rietveld fit to neutron and synchrotron x-ray powder diffraction data in the orthorhombic *Pmmm* space group, with cell parameters $a=3.9223(3)$ Å, $b=3.9360(3)$ Å, $c=11.7073(8)$ Å, and $V=180.74(2)$ Å^3 (room temperature). Antiferromagnetic ordering of Cu and Co magnetic moments is observed below 205(4) K. The magnetic structure with cell $a_M=2a$, $b_M=2b$, and $c_M=2c$, could be described with the Shubnikov space group $Fmmm'$. The magnetic moments of both equivalent Cu/Co sites were determined at 50 and 170 K to be $0.83(3)\mu_B$ and $0.58(3)\mu_B$, respectively, consistent with one unpaired electron per atom. The fit of the intensities to a simple mean field magnetic model appeared to be insufficient to account for the variation of moments at temperatures close to T_N while a three dimensional Heisenberg model could improve the fit. Susceptibility measurements between 4 and 350 K also show irreversibility below 150 K. The local environments of Cu and Co were studied by extended x-ray absorption fine structure spectroscopy at both absorption edges. Cu atoms adopt an elongated octahedral or square-based pyramidal oxygen environment which suggests mainly the presence of Cu(II) in the structure. Co adopts different local environments, depending on the electronic and spin states.

DOI: 10.1103/PhysRevB.71.144405 PACS number(s): 75.25.+z, 61.12.−q, 61.10.Ht

I. INTRODUCTION

Oxygen-deficient perovskites are lamellar oxides with strong correlations between structure, magnetic and transport properties.[1–3] The strong overlap of the unfilled 3*d* electron orbitals of the transition metal atoms with the oxygen 2*p* orbitals plays a key role in the behavior of these oxides. As a consequence many physical properties such as high T_c superconductivity, colossal magnetoresistivity and piezoelectricity are noted. The importance of these properties has justified the extensive work performed on these systems.

The $R\mathrm{Ba}M1M2\mathrm{O}_{5+\delta}$ series (R=rare earth or yttrium, $M1, M2$=transition metal ions) has been widely studied since it involves the presence of two layers, $M1\mathrm{O}_2$ and $M2\mathrm{O}_2$, where it is possible to combine different kinds of transition metal atoms, in an ordered or disordered network. The first studied system was $YBaCuFeO_5$ (YBCFO), due to the structural similarity to the high T_c superconductor YBCO.[4–10] The $R\mathrm{BaCuFeO}_5$ system (RBCFO) has shown very interesting magnetic properties, dependent on the rare earth (RE) atom size.[11–16] Thus, incommensurate and commensurate antiferromagnetic superstructures have been reported for YBCFO and for TmBCFO and LuBCFO, respectively. At the other extreme, LaBCFO showed a body centered orthogonal structure—a pseudocubic model—with the same occupation site for lanthanum and barium that yielded a magnetic structure differing from the other members of the series. Still another system of interest is the $R\mathrm{BaCuCoO}_{5+\delta}$ series. This series presents the attractive combination of cobalt and copper oxygen layers, where the spin states and magnetic ordering of a cobalt structure could be studied in the presence of a cuprate network.

The study of cobalt oxides has attracted additional interest due to the existence of various spin states for a given oxidation state.[17–30] The reason for this is the similar values of the intra-atomic exchange energy (J_H) and the crystal field splitting (Δ_{cf}) due to the octahedral and pyramidal environments. Thus, thermal effects are very important for the spin states present in these systems, since the electronic configuration in these 3*d* orbitals is very much temperature dependent.

Cobalt in these oxygen-deficient perovskites is mainly in the Co(III) oxidation state. The possible spin states are then as follows:[4–7] Low spin (LS) $t_{2g}^6 e_g^0$ ($S=0$); intermediate spin (IS) $t_{2g}^5 e_g^1$ ($S=1$), and high spin (HS) $t_{2g}^4 e_g^2$ ($S=2$). At low temperature, the LS and IS states are energetically more favorable, and transitions from LS to IS and IS to HS are expected upon warming. $YBaCuCoO_5$ (YBCCO), the prototype of the RBCCO series, is an antiferromagnetic insulator and crystallizes in the tetragonal space group $P4/mmm$, with $T_N=536(3)$ K, $\mu=1.49(2)\mu_B$ [room temperature (RT)] and its magnetization follows a simple mean field model.[31]

A systematic structural and magnetic study of $R\mathrm{BaCuCoO}_{5+\delta}$ compounds (R=La, Pr, Nd, Sm, Eu, Dy, Er, and Tm) has been performed using synchrotron x-ray and neutron powder diffraction, magnetic susceptibility, and extended x-ray absorption fine structure (EXAFS) spectroscopy techniques. The present work reports the crystal and magnetic structure of $LaBaCuCoO_{5+\delta}$, with an unusually high

nonstoichiometric oxygen content, $\delta \approx 0.6$, LaBCCO, in the temperature range 7.5–300 K. The structure and magnetism of the other members of the series will be published elsewhere.

II. EXPERIMENTS

The preparation of the sample was performed by the standard solid state reaction technique. La_2O_3 (99.9%, Aldrich), CuO (99.9%, Aldrich), $BaCO_3$ (99%, Sigma), and $Co_3O_{4.026(1)}$ (nominal Co_3O_4, 99.9%, Sigma, exact Co content determined by atomic absorption analysis) were ground together in stoichiometric amounts. Pellets of the resulting powder were heated in air at 850 °C for 6 h for decarbonation and then heated at 950 °C for 24 h. Four additional steps of grinding and heating cycles in an open crucible were performed at 970 °C to achieve a pure sample. Purity was checked by conventional x-ray powder diffraction using a SEIFERT Scintag PAD II diffractometer with Cu $K\alpha$ radiation. The nonstoichiometric oxygen concentration was determined from a combined Rietveld refinement of neutron and synchrotron x-ray powder diffraction data. The neutron powder diffraction data were collected on the BT-1 32-detector neutron powder diffractometer at the NIST Center for Neutron Research.[32] The sample, with approximate weight 15 g, was transferred to a vanadium container (length 5.1 cm, o.d. 1.1 cm). The instrument settings were a Cu(311) monochromator with a wavelength of 1.5403(2) Å, a take-off angle of 90°, and in-pile collimation of 15 min of arc. The beam was masked to 5.1 cm $\times$ 1.1 cm at the sample. Data were collected for 8 h for each at $\approx$295, 50, and 170 K over the range $3 < 2\theta < 165$ degrees with a step size of 0.05°.

The synchrotron x-ray diffraction data were collected with a Huber six-axis diffractometer, in reflection geometry (Bragg-Brentano powder diffraction) using the instrument at the D12A-XRD1 station at the National Synchrotron Light Source (LNLS) in Campinas, SP, Brazil, working at 1.3 GeV and a nominal ring current between 100 and 250 mA. The energy of the incident radiation was fixed approximately at 9.67 keV to achieve maximum photon flux at the sample. The experimental wavelength and instrumental peak shape contributions were obtained from a Rietveld fit of a powder pattern of an yttria standard sample [$\lambda = 1.283\,26(6)$ Å]. Scans were performed between 0.5 and 9 $Å^{-1}$ at steps of 0.001 $Å^{-1}$ in q space with constant monitor counts per step, with total approximate collection time of 1 h. Magnetic order parameter measurements were performed at triple axis spectrometer BT-7 at NCNR,[32] between 7.5 and 250 K using a Ge(311) monochromator ($\lambda = 2.0775$ Å) in the $\theta - 2\theta$ scan mode. The diffracted intensity was collected for 10 min at steps of 5 K with the detector fixed at the maximum of the magnetic peak. After that, 11 scans of the peak were performed at different temperatures to confirm the consistency of the previous temperature scan and obtain integrated intensities to evaluate the evolution of the magnetic ordering.

The Rietveld refinements were performed using the GSAS/EXPGUI suite of programs[33,34] applying the Thompson, Cox and Hastings modified pseudo-Voigt peak shape function and a shifted-Chebyshev polynomial for background description. A neutron absorption correction was applied using a computed value of $\mu \cdot R/\lambda$ and the Lobanov and Alte da Veiga correction function implemented in the same package. Anomalous scattering factors for x-ray were taken from the web site: www.bmsc.washington.edu/scatter/AS_index.html and checked with the FPRIME[35] program.

X-ray absorption spectra at the Cu K and Co K absorption edges were collected at room temperature in transmission mode on the XAS beam line at LNLS. Four spectra, each taking about 30 min, were averaged to give the final data sets.

The EXAFS data were analyzed in the standard way using the IFEFFIT[36] suite of programs. This analysis included the normalization of the extended fine structure to the absorption edge step energy and height, removal of a nonoscillatory background curvature, conversion to photoelectron wave vector (k) space, and Fourier transformation (FT) to radial (r) coordinates. The peaks were Fourier filtered and back-transformed into k space. La_2CuO_4 and $LaCoO_3$ were used as reference compounds to analyze the Cu K and the Co K edges spectra, respectively. The bond lengths derived from the neutron powder diffraction analysis discussed in this paper were used to generate the paths for the analysis. The regions selected for filtering were 1.4–2.5 Å and 1.4–2.7 Å, for Co and Cu, respectively.

The evolution of magnetic properties with temperature was followed using a Quantum Design superconducting quantum interference device (SQUID) magnetometer.

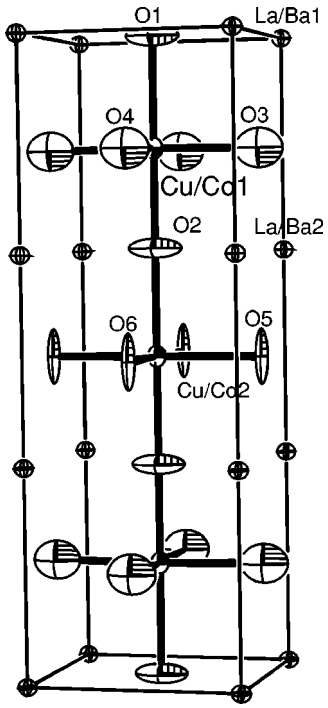

FIG. 1. (Color online) ORTEP view of one unit cell of $LaBaCuCoO_{5.6}$ at room temperature in the *Pmmm* space group with labeling scheme. Ellipsoids are shown with 60% probability. Note that O1 and O2 atoms display occupancies lower than unit so the octahedral coordination of Cu/Co atoms could be pyramidal in many cases.

TABLE I. Final structural parameters for the refinement of LBCCO at RT.

Space group: *Pmmm*, $a=3.922\,31(30)$ Å, $b=3.935\,97(33)$ Å, $c=11.7073(8)$ Å, $V=180.739(24)$ Å^3

Atom	Site	x	y	z	$U_{eq}(10^{-2}$ Å$^2)$[a]	SOF
La1	1*a*	0	0	0	1.26	0.255(31)
Ba1	1*a*	0	0	0	1.26	0.745(31)
La2	2*q*	0	0	0.3373(4)	1.26	0.623(16)
Ba2	2*q*	0	0	0.3373(4)	1.26	0.377(16)
Cu1	2*t*	0.5	0.5	0.1747(8)	1.12	0.437(11)
Co1	2*t*	0.5	0.5	0.1747(8)	1.12	0.563(11)
Cu2	1*h*	0.5	0.5	0.5	1.12	0.626(21)
Co2	1*h*	0.5	0.5	0.5	1.12	0.374(21)
O1	1*f*	0.5	0.5	0	4.18	0.975(20)
O2	2*t*	0.5	0.5	0.3305(11)	4.18	0.719(12)
O3	2*s*	0.5	0	0.1770(26)	4.26	1
O4	2*r*	0	0.5	0.1774(26)	4.26	1
O5	1*d*	0.5	0	0.5	3.17	1
O6	1*g*	0	0.5	0.5	3.17	1

δ value (based on $LaBaCuCoO_{5+\delta}$)$=0.61(3)$

Global Rwp$=7.78\%$, Rp$=4.96\%$, $\chi_r^2=1.984$ for 61 variables

[a]U_{eq}=one-third of the orthogonalized U_{ij} tensor.

III. RESULTS

The crystal structure fitting for LaBCCO was performed by joint neutron and synchrotron x-ray data refinement at room temperature. The major high angle peaks ($2\theta>20°$) of the neutron powder pattern and all the peaks in the x-ray pattern could be indexed in a cubic unit cell with $a_P \approx 3.91$ Å but the typical *Pm*-3*m* disordered oxygen-deficient perovskite structural model was not able to index all the neutron diffraction intensities. The presence of a very small peak at $2\theta\approx 7.5°$ ($d=11.7$ Å) in the neutron pattern indicated a likely superstructure with $c\approx 3a_P$ since there is no $\lambda/3$ component in the neutron beam. Both powder patterns were then indexed in a tetragonal cell $a\approx b\approx a_P$ and $c\approx 3a_P$. The tripled cubic structural model proposed is similar to the one found for the $La_{1.5}Ba_{1.5}Cu_3O_{7+\delta}$ compound.[37,39–41] The atomic positions in the tetragonal *P*4/*mmm* structure proposed for that compound are Ba: 2*h* [$z\approx 0.18$, SOF (site occupation factor)$=0.75$], La: 1*d* and 2*h* ($z\approx 0.18$, SOF$=0.25$), Cu: 1*a* and 2*g* ($z\approx 0.35$), O: 2*g* ($z\approx 0.16$), 4*i* ($z\approx 0.37$), 2*f* (SOF≈ 0.7) and 1*b* (SOF ≈ 0.1). Applying the same model to the $LaBaCuCoO_{5+\delta}$ formula leads to the possible substitution of the whole Cu: 1*a* and 0.25 Cu: 2*g* sites with Co, or half of Cu atoms in each site.

The initial refinements with the first substitution rapidly showed that the symmetry of the network must still be lowered, as some very small peaks in the neutron diffraction pattern remained unindexed. Further, site segregation for Co and oxygen vacancies was suspected.

A symmetry decrease to the orthorhombic *Pmmm* space group with a shift of origin to the tetragonal 2*h* position leads to the final structural model shown in Fig. 1. The atomic coordinates, occupancies (SOF), and thermal parameters, together with nonstructural parameters and residuals, are shown in Table I and the fitted patterns in Fig. 2.

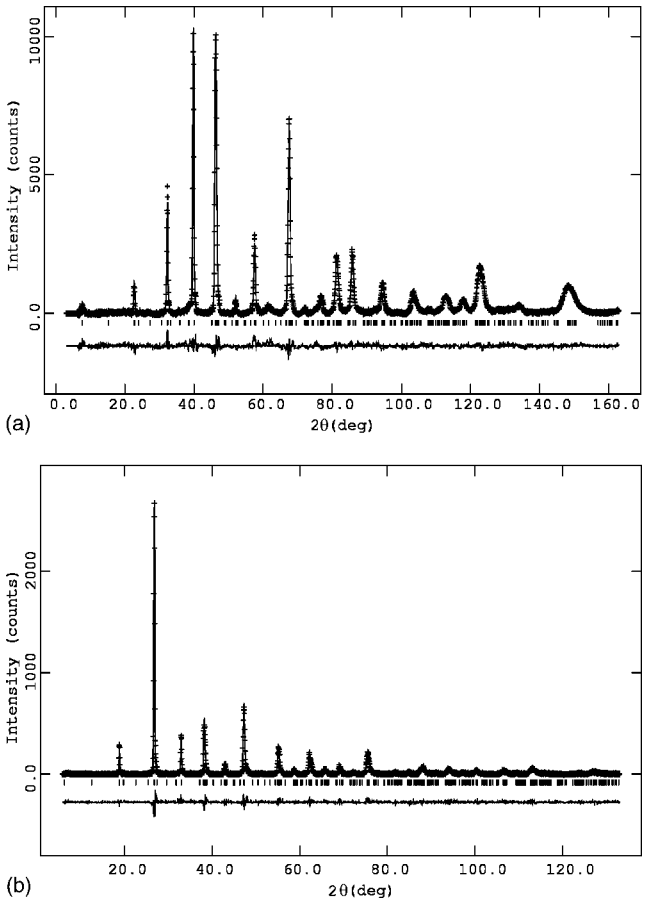

FIG. 2. (Color online) NPD (a) and SXPD (b) patterns of LBCCO fitted by the Rietveld method with the *Pmmm* structural model described in Table I using GSAS/EXPGUI suite of programs.

The site occupancy for La/Ba and Cu/Co pairs were refined in order to find a possible ordering of cations in the structure, as observed in $La_{1.5}Ba_{1.5}Cu_3O_{7+\delta}$.[37] The results are not conclusive due to the appreciable correlation between the SOF and thermal parameters. The oxygen content derived from the refinement of the O1 and O2 occupancies [$\delta=0.61(3)$] yields a mean oxidation state of the (Cu/Co) pair of 3.11+. This could be achieved with the complete or partial oxidation of Cu(II) into Cu(III) or Co(III) into Co(IV).

The Cu/Co-O bond distances are shown in Table II. These bond distances are consistent with those observed in $La_{1.5}Ba_{1.5}Cu_3O_{7+\delta}$, where, depending on δ, the amount of Cu(III) could increase to one-third of the total atoms.[37]

The typical square-planar conformation of Cu(III) expected in this structure can only occur when oxygen vacancies are paired at both Cu apical sites. This could only be achieved at the 1*h* site, where the probability of finding an oxygen deficiency above and below is higher, as the O2 oxygen occupancy for each 2*t* sites is 0.78, in comparison to the 0.98 occupancy for the 1*c* site. However, the presence of a symmetric octahedral Cu(III) environment as in $LaCuO_3$ (Ref. 38) cannot be ruled out.

TABLE II. Selected bond distances from Rietveld refinement of LBCCO at RT (Å).

Cu/Co(1)-O(1)	2.036(9)	Cu/Co(2)-O(2)	1.986(12)
Cu/Co(1)-O(2)	1.823(9)	Cu/Co(2)-O(5)	1.964 98(19)
Cu/Co(1)-O(3)	1.9653(6)	Cu/Co(2)-O(6)	1.958 33(16)
Cu/Co(1)-O(4)	1.9586(6)		

Another feature that should be mentioned is the relatively wide peaks observed in this sample, both by neutron or synchrotron x-ray diffraction. This peak width should come from a wide range of *d*-spacings in each cubic direction, allowing different $1\times1\times n$ cells to be consistent with them.

Two factors lead to the appearance of pseudoextinctions in the x-ray diffraction pattern. Since the La/Ba and Cu/Co pairs have nearly identical x-ray scattering power with $f_{Ba/La}\approx 2f_{Cu/Co}$ ($Z_{Co}=27$, $Z_{Cu}=29$, $Z_{Ba}=56$, and $Z_{La}=57$), diffraction intensities are approximately zero for several reflection classes. This also leads the 001 reflection to be very weak for the $1\times1\times3$ cell; the structure factor is dependent on the difference between populations of the O1, O2, and O3/O4 sites, which are nearly the same. For this reason the x-ray indexing is insensitive to the choice of *c* axis length, while the neutron pattern can only be indexed with a $1\times1\times3$ supercell.

An alternate explanation, that the phase $La_3Ba_3Cu_6O_{14+\delta}$, could be regarded as a mixture of phases of variable composition, was offered by Domenges *et al.*[42] We feel that this is improbable in this system due to the consistency between the structural results obtained with different sample preparation batches and different synthetic techniques. Moreover, a recent study by Ruiz-González *et al.*[43] describes the intergrowth of $1\times1\times2$ and $1\times1\times3$ oxygen deficient perovskite type layers in the $LaBaCuCoO_{5.2}$ sample during reduction to $LaBaCuCoO_{4.4}$ based on electron diffraction, HREM and powder diffractometry (for the composition $LaBaCuCoO_{5.2}$). They have refined the LaBCCO structure in a $1\times1\times5$ tetragonal $P4/mmm$ unit cell with $a=3.9352(3)$ Å and $c=19.539(2)$ Å based on a conventional x-ray diffraction pattern. An increase in the oxygen content, as in our sample, could lead to the stabilization of the $1\times1\times3$ layers, over the $1\times1\times2$. We see no evidence of peaks belonging to a $1\times1\times5$ phase in the neutron or synchrotron x-ray powder diffraction diagrams.

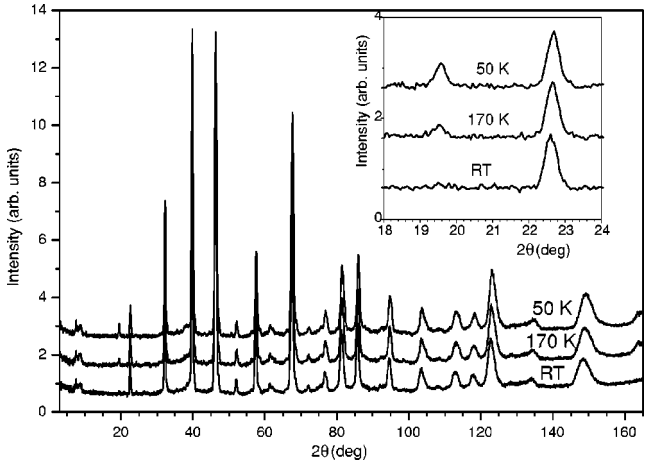

FIG. 3. (Color online) NPD patterns collected at 50 and 170 K, and RT, the evolution of the intensity of the magnetic peak at $2\theta=19°$ is shown in the inset.

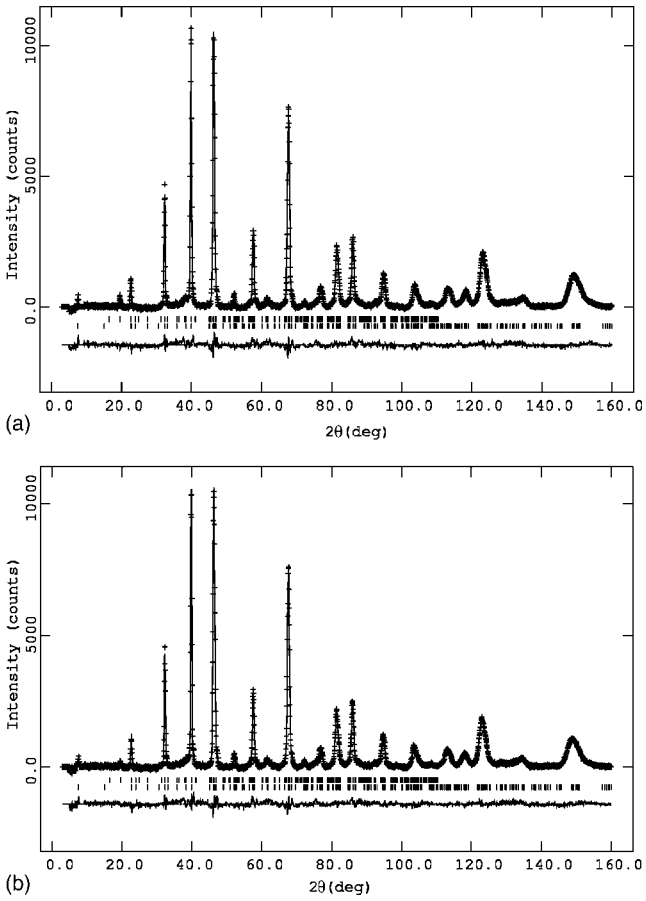

FIG. 4. (Color online) Fitted NPD patterns for $LaBaCuCoO_5$ at (a) 50 and (b) 170 K with a magnetic model $Fmmm^*$. Upper vertical lines show magnetic peak positions while lower vertical lines represent peak positions for the nuclear model.

The neutron powder patterns collected at 50 and 170 K show the presence of two peaks, at $2\theta\approx19.5°$ ($d\approx4.52$ Å) and $2\theta\approx38°$ ($d\approx2.32$ Å) that are absent at RT and whose intensity decays with temperature as is shown in Fig. 3. A long range magnetic ordering of Cu and Co atomic moments was proposed to explain the position and change in intensity of both peaks. Two different magnetic models are consistent with these peaks. Use of a magnetic cell with $a_M=b_M\approx\sqrt{2}a_p$ and $c_M\approx2a_p$ indexes these reflections as the $(101)_M$ and $(211)_M$ reflections. This magnetic cell is consistent with the pseudo-cubic structural model. An alternate model treats the lowering of the nuclear symmetry by doubling the orthorhombic $Pmmm$ $1\times1\times3$ cell to obtain an orthorhombic face-centered cell. This indexes the magnetic reflections as $(113)_F$ and $(313)_F$. In both cases the magnetic ordering is consistent with an antiferromagnetic *G*-type arrangement, where the six closest neighbors of each magnetic atom have a moment opposite to the central one. If the cubic model is

TABLE III. Final structural parameters and residuals of the NPD patterns at 50 and 170 K.

	Temperature (K)	50	170
Cell parameters	a (Å)	3.9148(5)	3.9167(5)
	b (Å)	3.9266(6)	3.9296(5)
	c (Å)	11.6809(11)	11.6900(11)
	V (Å^3)	179.56(6)	179.92(6)
Atom (site)	Parameter		
La1 (1a)	U_{eq}(10^{-2} Å^2)[a]	2.03	2.27
	SOF	0.42(6)	0.40(6)
Ba1 (1a)	U_{eq}(10^{-2} Å^2)[a]	2.03	2.27
	SOF	0.58(6)	0.60(6)
La2 (2q)	z	0.3389(7)	0.3387(7)
	U_{eq}(10^{-2} Å^2)[a]	2.03	2.27
	SOF	0.542(28)	0.551(27)
Ba2 (2q)	z	0.3389(7)	0.3387(7)
	U_{eq}(10^{-2} Å^2)[a]	2.03	2.27
	SOF	0.458(28)	0.449(27)
Cu1 (2t)	z	0.1782(11)	0.1780(11)
	U_{eq}(10^{-2} Å^2)[a]	1.96	2.16
	SOF	0.466(15)	0.447(14)
Co1 (2t)	z	0.1782(11)	0.1780(11)
	U_{eq}(10^{-2} Å^2)[a]	1.96	2.16
	SOF	0.534(15)	0.553(14)
Cu2 (1h)	U_{eq}(10^{-2} Å^2)[a]	1.96	2.16
	SOF	0.569(30)	0.606(29)
Co2 (1h)	U_{eq}(10^{-2} Å^2)[a]	1.96	2.16
	SOF	0.431(30)	0.394(29)
O1 (1f)	U_{eq}(10^{-2} Å^2)[a]	3.84	3.96
	SOF	0.882(34)	0.864(32)
O2 (2t)	z	0.3314(14)	0.3315(13)
	U_{eq}(10^{-2} Å^2)[a]	3.84	3.96
	SOF	0.670(19)	0.664(18)
O3 (2s)[a]	z	0.1781(36)	0.1772(39)
	U_{eq}(10^{-2} Å^2)[a]	5.57	5.80
O4 (2r)[a]	z	0.1750(36)	0.1752(40)
	U_{eq}(10^{-2} Å^2)[a]	5.57	5.80
O5 (1d)[b]	U_{eq}(10^{-2} Å^2)[a]	3.72	4.03
O6 (1g)[b]	U_{eq}(10^{-2} Å^2)[a]	3.72	4.03
	δ (for $LaBaCuCoO_{5+\delta}$)	0.48(5)	0.46(5)
	μ Cu/Co site (μ_B)	0.828(29)	0.557(34)
	Residuals		
	R_{wp} (%)	5.81	5.43
	Rp (%)	4.74	4.41
	χ^2_r (# of parameters)	3.905 (46)	3.322 (46)
	R_B/R_M (%)	8.81/38.47	7.80/42.56

[a]U_{eq}=one-third of the orthogonalized U_{ij} tensor.
[b]Fully occupied O sites (SOF=1).

TABLE IV. Structural parameters obtained from the EXAFS analyses using La_2CuO_4 and $LaCoO_3$ as references. Δk (Å^{-1}) =3–12. Models ×3 and ×2 correspond to the $a\times a\times 3a$ to the $a\times a\times 2a$ unit cells, respectively.

Model	Bonding	Site 1	N	R (Å)	$10^3\Delta\sigma^2$ (Å^2)	Occupancy
×3	Co-O	1	2	2.0	1	0.8
		1	2	2.0		
		1	0.7	2.1		
		1	0.7	2.1		
	Co-O	2	2	1.8	1	0.2
		2	2	1.8		
		2	1.4	2.0		
×2	Co-O		1.0	2.0	4	
			2	2.0		
			2	2.0		
×3	Cu-O	1	2	1.9	0.7	Undetermined
		1	2	1.9		
		1	1.9	2.2		
	Cu-O	2	2	1.9	4	Undetermined
		2	2	1.9		
		2	1.9	2.1		
×2	Cu-O		2	1.9	1	
			2	1.9		
			1.8	2.2		

considered, then the magnetic structure could be modeled with the aid of the Shubnikov space group $I4'm'm$ (No. 229) (Ref. 44) while if the orthorhombic model is considered the $Fmmm'$ (No. 523) space group should be used. In the first case one independent Cu/Co position results, but in the second one, two independent positions with opposite magnetic moments are needed, as in the respective nuclear models. Both of the cases lead to the same result, so the $Fmmm'$ one was considered, as it was the simplest to combine with the $Pmmm$. A second phase with $a^i_M=2a^i_N$ with only magnetic scatterers was included in the refinement of the NPD patterns obtained at 50 and 170 K in order to model the magnetic peaks. Cell parameters, coordinates, and U_{ij} of the Cu and Co nuclear and magnetic contributions were constrained conveniently in both phases and the magnetic moments of both positions were refined keeping equal modulus and opposite directions. The fitted patterns are shown in Fig. 4 and the final coordinates and magnetic moments of magnetic sites are shown in Table III.

The magnetic moments of both Cu/Co sites in the $Pmmm$ model converged to $0.83(3)\mu_B$ and $0.58(3)\mu_B$ at 50 and 170 K, respectively. This implies that a maximum of one unpaired electron per magnetic site should be present (considering a typical spin-only contribution for 3d cations).

The main results obtained from the EXAFS analysis are presented in Table IV. The FTs and the inverse FTs for the $1\times1\times3$ and $1\times1\times2$ cells, for Co K and Cu K are shown in Figs. 5 and 6, respectively. As can be deduced from these figures, the Co environment has significantly improved with the existence of two different sites as in $a\times a\times 3a$ case. The

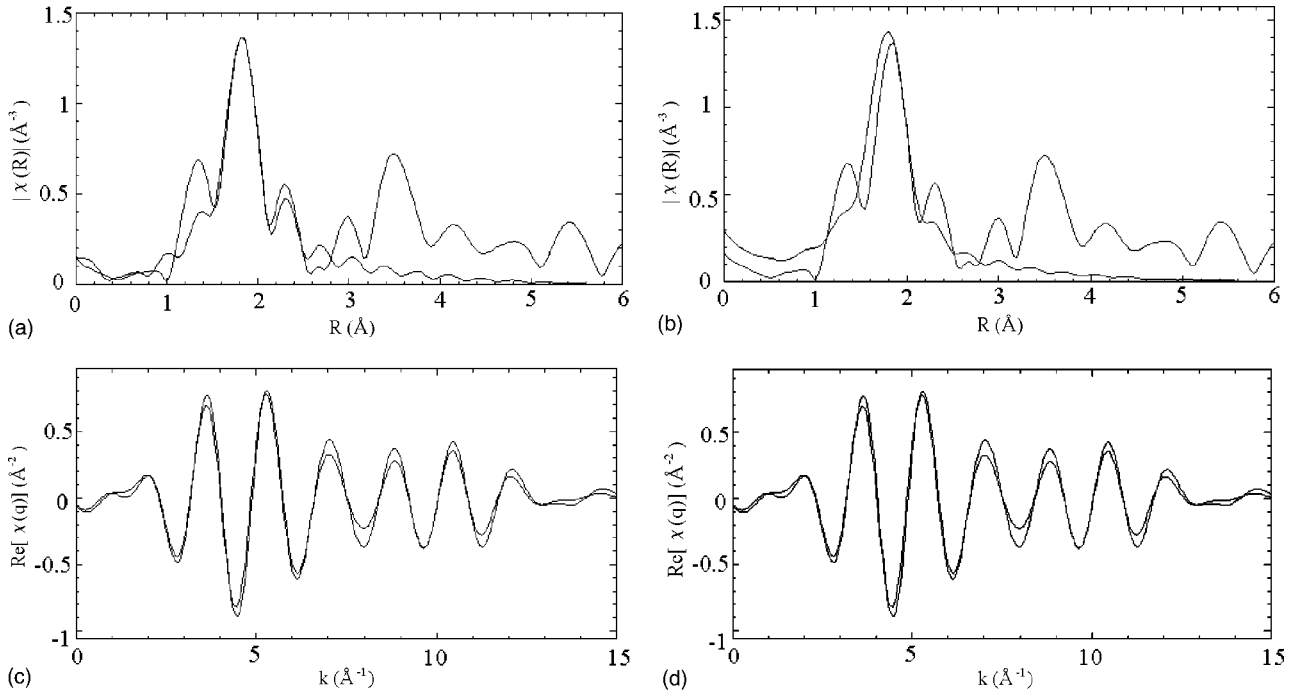

FIG. 5. (Color online) The FTs of raw EXAFS and of the fit of $k^2\chi$(k) for Co *K* according to (a) the $a\times a\times 3a$ and (b) the $a\times a\times 2a$ models. The inverse FTs $k^2\chi$(k) for Co *K* according to (c) the $a\times a\times 3a$ and (d) the $a\times a\times 2a$ models (blue and red line, experimental data and model fit, respectively).

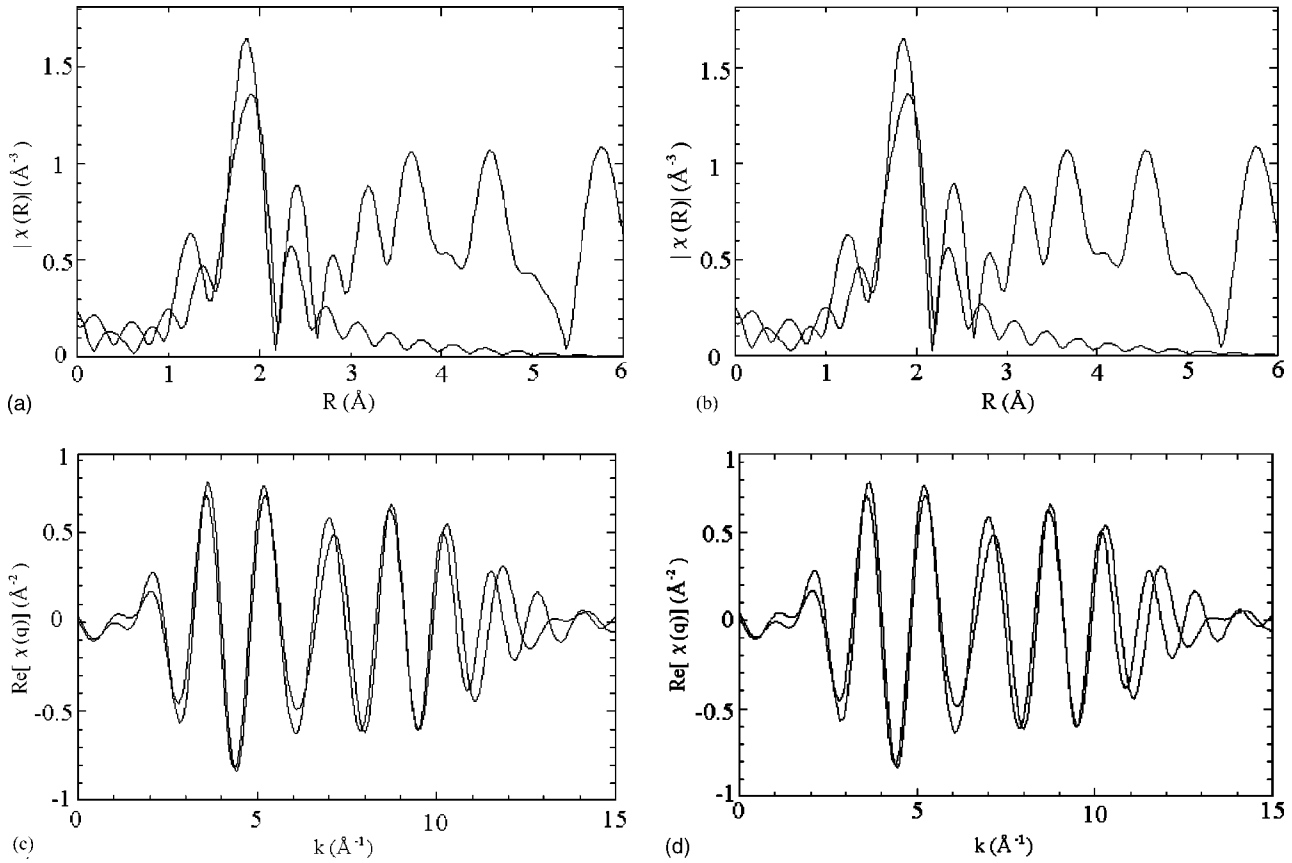

FIG. 6. (Color online) The FTs of raw EXAFS and of the fit of $k^2\chi$(k) for Cu *K* according to (a) the $a\times a\times 3a$ and (b) the $a\times a\times 2a$ models. The inverse FTs $k^2\chi$(k) for Cu *K* according to (c) the $a\times a\times 3a$ and (d) the $a\times a\times 2a$ models (blue and red line, experimental data and model fit, respectively).

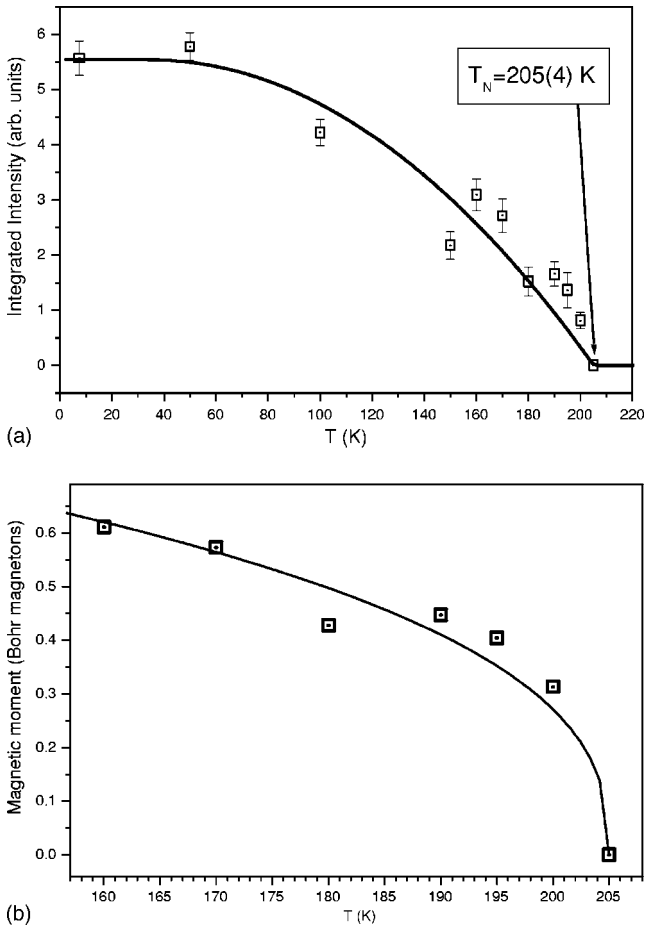

FIG. 7. (Color online) (a) Integrated intensity of the $(101)_M$ peak as a function of temperature from 7.5 to 205 K with a mean-field model fit. (b) LS-fit of the exponential function $\mu=\mu_0^*(T-T_N)^\beta$ to the integrated intensities close to the transition temperature with $\beta=0.376$ fixed for a Heisenberg 3D critical model [$\mu_0=1.10(4)\mu_B, T_N-205.04(4)$ K].

Cu environment, however, does not exhibit any difference. Moreover, the EXAFS analysis for Cu shows two sites for the $a\times a\times 3a$ model that converged practically to the same environment, and this result has been obtained for the $1\times 1\times 2$ model as well. For this reason the occupancy for each site could not be unambiguously determined. The coordination sphere is then an elongated octahedron, in agreement with the one expected for the Jahn-Teller ion Cu(II) ([Ar]$3d$;^{9} $S=1/2$), not a symmetric environment as would correspond to the non-Jahn-Teller Cu(III) ([Ar]$3d$;^{8} $S=0$). This fact suggests that Cu is mainly Cu(II) in LaBCCO. The convergence to a one-site model for Cu reveals that the inclusion of cobalt in the structure is vital for the occurrence of the triple cell observed in LaBCCO. This would explain why this triple cell is not observed in the related compound $LaBaCuFeO_5$.[11,12] The probability that different spin states for both possible oxidation states in Co coexist in LaBCCO, could be the reason for the better fit in this double-site triple-cell model.

The electronic and spin configurations of Co(III) **(**[Ar]$3d$;^{6} low spin (LS), $S=0$, intermediate spin (IS), $S=1$, or high spin (HS), $S=2$**)** and Co(IV) ([Ar]$3d$;^{5} low spin $S=1/2$, intermediate spin $S=3/2$ or high spin $S=5/2$) suggest not only different ionic sizes (arising from different oxidation states), but also the possibility of Jahn-Teller and non-Jahn-Teller ions, which could be better fit with a double-site model.

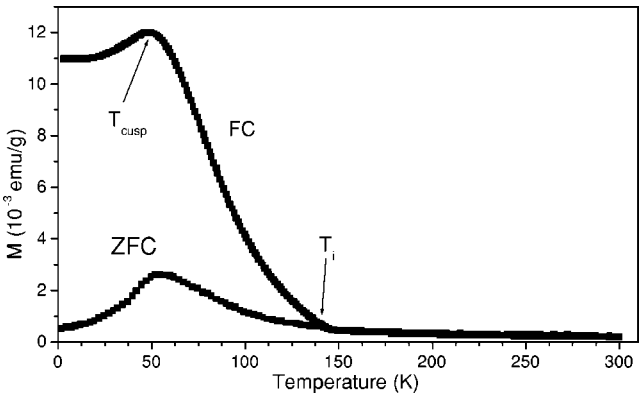

FIG. 8. (Color online) FC (high) and ZFC (low) branches of the magnetic susceptibility of $LaBaCuCoO_{5.6}$.

The analysis of the electronic and spin configurations of Cu(II), Cu(III), Co(III), and Co(IV), together with the consideration that the mean Cu/Co site valence should be close to 3+ (obtained from the value of the nonstoichiometric oxygen content $\delta\approx 0.5$) indicates that two possible electronic and spin configurations of Cu and Co more accurately describe the magnetic behavior at low temperatures.

There are two possible models that agree with the low temperature neutron diffraction data refinements: Cu(II)/low spin-Co(IV) (each $S=1/2$), or Cu(III)/intermediate spin-Co(III) (copper $S=0$ and cobalt $S=1$). In both cases there is one unpaired electron per site. Based on the results obtained from the EXAFS analysis, the first configuration seems to be most significant. Of course the possibility that both configurations coexist with different proportions in the compound cannot be ruled out. In order to maintain charge balance, Cu(III) ($S=0$) and Co(III)—probably in the low temperature stable LS configuration ($S=0$)—could also be present, thus, not contributing to the magnetic moment.

The evolution of the integrated intensity of the $(101)_M$ reflection with temperature is shown in Fig. 7(a). This allows the ordering temperature to be determined as $T_N=205(4)$ K. This variation could be fitted by means of simple mean field model, where the only interaction between the magnetic ions is the effective field due to the neighbors. Generally a mean field model does not describe the intensities near T_N accurately, but with powder data the deviations are difficult to determine unambiguously. The fit of a power law, consistent with a Heisenberg 3D, to the mean magnetic moment of the Cu/Co atoms, for temperatures above 150 K is shown in Fig. 7(b). The presence of a significant depression in the $I(101)_M$ vs T curve, near $T=150$ K could be related with the features observed in the zero field cooled (ZFC) and field cooled (FC) magnetization curves shown in Fig. 8. The evolution of the FC inverse magnetization with temperature is also shown in Fig. 9. A very remarkable irreversible behavior can be observed at temperatures below the irreversible temperature, $T_i=142(2)$ K. A cusp is observed at 52(2) K for

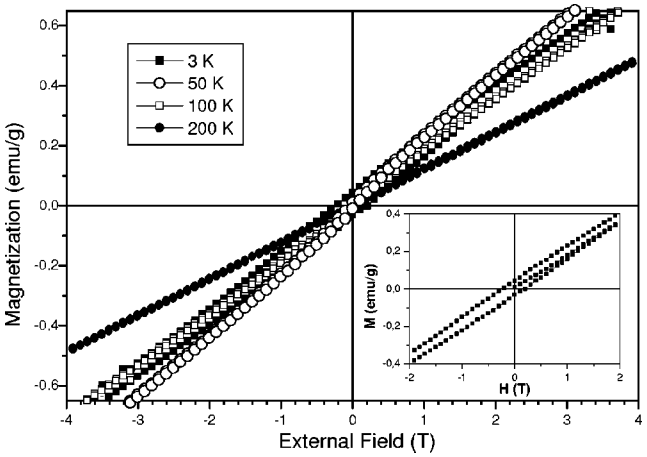

FIG. 9. (Color online) M vs H measurements at different temperatures for LaBCCO. The inset shows the details of the hysteresis at 3 K.

both branches, ZFC and FC. The FC curve shows strong—but not pure—ferromagnetic character, with a very pronounced increase with decreasing temperature, just with the maximum at the cusp to show an antiferromagnetic contribution. The ZFC curve shows antiferromagnetic behavior but with a maximum not coincident with the Nèel temperature, $T_N=204(3)$ K. The difference in the magnetization between FC and ZFC curves is related to the energy involved in the alignment of magnetic domains. From the Curie-Weiss fit of the inverse magnetization curve above $T_N=204$ K the value of the Weiss temperature (θ) was determined as $-31(1)$ K—as expected for AF interactions—and the effective magnetic moment was $2.66(2)\mu_B$. This value could be explained by the presence of Cu(II) ($S=1/2$) and Co(IV) IS and possibly HS ($S=3/2$ and $5/2$, respectively), calculated on the basis of a spin-only situation. Thus, the collapse of the magnetic ordering in the network could be accompanied by a change in the spin configuration of Co.

Figure 9 shows the magnetic hysteresis of LaBCCO. The magnetization is not saturated even at 5 T. When this feature is observed in these perovskite systems, the accepted explanation is generally stated through the paramagnetic contribution from the rare earth ion. However, since La^{3+} is a non-magnetic ion, in this case this explanation cannot be invoked. The inset in Fig. 9 shows the low field portion of the hysteresis loop at 3 K.

IV. CONCLUSIONS

The results presented in this report indicate that the structure of $LaBaCuCoO_{5.6}$ can be described as a pseudocubic oxygen-deficient perovskite structure $ABO_{3-\delta}$ where Cu(II) and Co(IV) cations occupy the B site and La and Ba the A ones randomly. The oxygen vacancies could be modeled to be partially ordered in a $1\times1\times3$ orthorhombic model, consistent with some previous results. The EXAFS analysis shows that the environment surrounding the cobalt ions can be better described with this triple-cell model, while the copper coordination sphere clearly indicates that a single site is enough to obtain a reliable picture. The ordering of 3d cations produces a G-type magnetic arrangement. There is a strong magnetic irreversibility in the system at temperatures below $T\approx150$ K. This phenomenon could have some effect on the long range magnetic ordering. The evolution of the integrated intensity of $(101)_M$ with temperature could suggest the existence of a transition at 150 K.

The likely presence of Co(IV) in different electronic state configurations appears to play a key role in the structural and the magnetic behavior of LaBCCO.

ACKNOWLEDGMENTS

L.S. and A.W.M. wish to thank LNLS, Brazil and NIST, USA for the provision of synchrotron and neutron beam time, respectively. This work was partially supported by PEDECIBA (through a Ph.D. grant), CONICYT-FCE (Grant No. 6046) and CSIC—Uruguayan organizations—and FAPESP, CNPq, and National Synchrotron Light Source (LNLS) under proposal D12A-XRD1-1588-Brazilian organizations. A.W.M. wishes to thank Dr. G. Azevedo and Dr. S. Kycia for their help with the data collection. Certain commercial products are identified to document experimental procedures. Such identification is not intended to imply recommendation or endorsement by the National Institute of Standards and Technology, nor is it intended to imply these products are necessarily the best available for the purpose.

*Corresponding author.

[1] L. Er-Rakho, C. Michel, P. Lacorre, and B. Raveau, J. Solid State Chem. **73**, 531 (1988).

[2] C. Meyer, F. Hartmann-Boutron, Y. Gros, and P. Strobel, Solid State Commun. **76**, 163 (1990).

[3] Y. K. Atanassova, V. N. Popov, G. G. Bogachev, M. N. Iliev, C. Mitros, V. Psycharis, and M. Pissas, Phys. Rev. B **47**, 15 201 (1993).

[4] A. W. Mombrú, C. Christides, A. Lappas, K. Prassides, M. Pissas, C. Mitros, and D. Niarchos, Inorg. Chem. **33**, 1255 (1994).

[5] V. Caignaert, I. Mirebeau, F. Bouree, N. Nguyen, A. Ducouret, J. M. Greneche, and B. Raveau, J. Solid State Chem. **114**, 24 (1995).

[6] A. W. Mombrú, K. Prassides, C. Christides, R. Erwin, M. Pissas, C. Niarchos, and D. Mitros, J. Phys.: Condens. Matter **10**, 1247 (1998).

[7] M. Ruiz-Aragón, U. Amador, E. Morán, and N. H. Andersen, Physica C **235–240**, 1609 (1994).

[8] M. Pissas, C. Mitros, G. Kallias, V. Psycharis, D. Niarchos, A. Simopoulos, A. Kostikas, C. Christides, and K. Prassides, Physica C **185**, 553 (1991).

[9] M. Pissas, C. Mitros, G. Kallias, V. Psycharis, A. Simopoulos, A. Kostikas, and D. Niarchos, Physica C **192**, 35 (1992).

[10] L. Er-Rakho, C. Michel, F. Studer, and B. Raveau, J. Phys. Chem.

Solids **48**, 377 (1977).
[11] H. Pardo, W. A. Ortiz, F. M. Araújo-Moreira, L. Suescun, B. Toby, E. Quagliata, C. A. Negreira, K. Prassides, and A. W. Mombrú, Physica C **313**, 105 (1999).
[12] A. W. Mombrú, H. Pardo, L. Suescun, B. H. Toby, W. A. Ortiz, C. A. Negreira, and F. M. Araújo-Moreira, Physica C **356**, 149 (2001).
[13] A. W. Mombrú, A. E. Goeta, H. Pardo, P. N. Lisboa-Filho, L. Suescun, R. A. Mariezcurrena, O. N. Ventura, R. Behak, K. H. Andersen, and F. M. Araújo-Moreira, J. Solid State Chem. **166**, 251 (2002).
[14] N. Guskos, V. Likodimos, J. Kuriata, H. Metz, W. Windsch, M. Wabia, C. Mitros, and D. Niarchos, Phys. Status Solidi B **181**, K 69 (1994).
[15] M. J. Ruiz-Aragón, E. Morán, U. Amador, J. L. Martínez, N. H. Andersen, and H. Ehrenberg, Phys. Rev. B **58**, 6291 (1998).
[16] M. Pissas, G. Kallias, V. Psycharis, H. Gamari-Seale, D. Niarchos, A. Simopoulos, and R. Sonntag, Phys. Rev. B **55**, 397 (1997).
[17] R. H. Potze, G. A. Sawatzky, and M. Abbate, Phys. Rev. B **51**, 11501 (1995).
[18] H. Takahashi, F. Munakata, and M. Yamanaka, Phys. Rev. B **57**, 15 211 (1998).
[19] E. Chappel, M. Holzapfel, G. Chouteau, and A. Ott, J. Solid State Chem. **154**, 451 (2000).
[20] A. Krimmel, M. Reehuis, M. Paraskevopoulos, J. Hemberger, and A. Loidl, Phys. Rev. B **64**, 224404 (2001).
[21] H. W. Brinks, H. Fjellvåg, A. Kjekshus, and B. C. Hauback, J. Solid State Chem. **147**, 467 (1999).
[22] M. Pouchard, A. Villesuzanne, and J. P. Doumerc, J. Solid State Chem. **162**, 282 (2001).
[23] M. Paraskevopoulos, J. Hemberger, A. Krimmel, and A. Loidl, Phys. Rev. B **63**, 224416 (2001).
[24] H. Nakatsugawa and E. Iguchi, J. Solid State Chem. **159**, 215 (2001); O. H. Hansteen, H. Fjellvåg, and B. C. Hauback, J. Solid State Chem. **141**, 411 (1998).
[25] F. Fauth, E. Suard, and V. Caignaert, Phys. Rev. B **65**, 060401(R) (2001).
[26] Q. Z. Huang, V. L. Karen, A. Santoro, A. Kjekshus, J. Lindén, T. Pietari, and P. Karen, J. Solid State Chem. **172**, 73 (2003).
[27] L. Barbey, N. Nguyen, V. Caignaert, M. Hervieu, and B. Raveau, Mater. Res. Bull. **27**, 295 (1992).
[28] I. A. Zaliznyak, J. M. Tranquada, R. Erwin, and Y. Moritomo, Phys. Rev. B **64**, 195117 (2001).
[29] J. Wu and C. Leighton, Phys. Rev. B **67**, 174408 (2003).
[30] M. R. Ibarra, R. Mahendiran, C. Marquina, B. García-Landa, and J. Blasco, Phys. Rev. B **57**, R3217 (1998).
[31] Q. Huang, P. Karen, V. L. Karen, A. Kjekshus, J. W. Lynn, A. D. Mighell, I. Natali Sora, N. Rosov, and A. Santoro, J. Solid State Chem. **108**, 80 (1994).
[32] The instrument is described in the NCNR web site (http://www.ncnr.nist.gov/).
[33] A. C. Larson and R. B. Von Dreele, Los Alamos National Laboratory Report No. LA-UR-86-748 (1987).
[34] B. H. Toby, EXPGUI, a graphical user interface for GSAS, J. Appl. Crystallogr. **34**, 210 (2001).
[35] R. B. Von Dreele (1994), Program FPRIME for Windows 1.0 for calculating real and anomalous x-ray dispersion coefficients.
[36] M. Newville and B. Ravel (2001), IFEFFIT suite of programs, version 1.0052.
[37] C. C. Torardi, E. M. McCarron, III, M. A. Subramanian, A. W. Sleight, and D. E. Cox, Mater. Res. Bull. **22**, 1563 (1987).
[38] G. Demazeau, C. Parent, M. Pouchard, and P. Hagenmueller, Mater. Res. Bull. **7**, 913 (1972).
[39] W. I. F. David, W. T. A. Harrison, R. M. Ibberson, M. T. Weller, J. R. Grasmeder, and P. C. Lanchester, Nature (London) **328**, 328 (1987).
[40] F. Izumi, H. Asano, T. Ishigaki, E. Takayama-Muromachi, Y. Matsui, and Y. Uchida, Jpn. J. Appl. Phys., Part 2 **26**, 1153 (1987).
[41] F. Izumi, E. Takayama-Muromachi, M. Kobayashi, Y. Uchida, H. Asano, T. Ishigaki, and N. Watanabe, Jpn. J. Appl. Phys., Part 2 **27**, 824 (1988).
[42] B. Domenges, M. Hervieu, C. Michel, A. Maignan, and B. Raveau, Phys. Status Solidi A **107**, 73 (1988).
[43] L. Ruiz-González, K. Boulahya, M. Parras, J. Alonso, and J. M. González-Calbet, Chem.-Eur. J. **8**(24), 5694 (2002).
[44] A. V. Shubnikov and N. V. Belov, *Colored Symmetry* (Pergamon Press, Oxford, 1964).